Effects of Nonlinear Distortion on Switched Multibeam FDMA Systems

Mattias Wennström Tommy Öberg and Anders Rydberg

Abstract

The effects of using an multicarrier amplifier (MCPA) in the transmit chain of a cellular FDMA system utilizing switched multibeam base-station antennas is investigated. By combining several carriers prior to amplification, the signal envelope will be time varying and the MCPA will introduce non-linear distortion of the amplified waveforms. It is shown how the main beam direction and frequency of any intermodulation product of any order can be calculated and a frequency allocation scheme is presented that reduces the intermodulation distortion at the mobile users. By Monte Carlo simulations, the probability distribution function of the received intermodulation distortion power is estimated, assuming a GSM system, as a function of the number of antenna elements and the number of active users. Comparisons with a one-element reference antenna is made, and it is shown that the received intermodulation distortion power for the users in the system is substantially reduced when the number of beams are increased or the user activity is reduced.

1 Introduction

Multibeam antennas are a viable choice for the implementation of the downlink (base-to-mobile) in wireless cellular communication systems due to the attractive trade-off between system performance and the complexity and cost of implementation [1],[2],[3]. The switched multibeam antenna has thus been the scope of several testbed and field trial investigations for its feasibility in GSM/FDMA networks [4],[5],[6],[7]. A multibeam antenna uses an array of antenna elements and has a beam-forming network that generates multiple narrow beams and a beam switching algorithm [8] of low-complexity which chooses (or switches) the downlink main beam simply in the direction where the strongest received signal [5],[9] comes from. In some implementations the downlink beamforming is performed entirely in hardware, thereby relaxing the signal processing requirements even further. Figure 1 shows an overview of the assumed transmitter architecture. In this implementation the downlink beam is selected in the digital signal processor, but the beamforming is performed in a beamforming network, implemented in hardware.

The multibeam technique is a common downlink beamforming method used in frequency division duplex (FDD) systems because the frequency duplex distance is typically significantly larger than the coherence bandwidth of the radio channel, which makes the uplink and downlink channel uncorrelated. However, the direction of arrival estimate of the uplink signal is still a useful estimate of the direction to the mobile at the downlink frequency [10].

Although switched-beam antennas significantly increases the carrier to interference ratio of the radio link [8], the drawback is the increased amount of hardware required at the base-station (BS) site. Each antenna and frequency channel in an FDMA system requires a single carrier power amplifier for the downlink transmission. Thus, to reduce size, cost and power consumption of the BS, multicarrier power amplifiers (MCPA) have been suggested for use in cellular systems [11]. For satellite systems, where small equipment size and low power consumption is of high importance, the combination of MCPA and array antennas has been utilized for a long time [12],[13],[14].

The co-amplification of several modulated signals with different center frequencies in an MCPA generates intermodulation distortion (IMD) due to the nonlinearity. The IMD is a substantial source of interference and must be included in the interference budget, although it has been shown that the IMD can be reduced by different linearisation techniques [15]. Some residual IMD power will however still be emitted by the antennas, and it is important to be able to predict this level to assure an acceptable system performance.

Not all IMD are harmful to the system however, since some parts of the distortion power can easily be removed by filtering. If $\{\omega_1, \ldots, \omega_M\}$ is the set of M center frequencies of the modulated carriers that enters the MCPA, some third order intermodulation products (IMP) in the output signal will be centered at the frequencies $2\omega_j$-ω_k and $\omega_j + \omega_k - \omega_l$. Thereby they fall onto other frequency channels that are used in the FDMA system and cannot be removed by filtering. Non-linearities in communication applications is most often modelled by considering only the third order IMP since the amplifiers operate well below the 1 dB compression point. In this region, the third order IMP dominates over higher order IMP so the distortion power from higher order IMP can safely be neglected.

The degree of a non-linearity is often measured by a two tone test, where two continuous wave (CW) tones with distinct frequencies are combined and connected to the input of the amplifier. The power of the IMP are measured in the output signal and the ratio to the power of the desired signal is calculated as a measure of the non-linearity. In third generation (UMTS) systems, the input signal has a 5 MHz bandwidth and a nonlinear amplifier will then introduce spectrum regrowth. Here the Adjacent Channel Leakage power Ratio (ACLR) is defined as the ratio of the transmitted power to the power measured after a receiver filter in the adjacent channels [16]. The receiver filter has a -3 dB bandwidth equal to the chip rate (3.84 MHz) in the 3GPP-standard of UMTS.

In a cellular system, the dominant IMD will come from the MCPA in the same cell, if the generated IMD falls onto other frequency channels used in that cell. Other examples of MCPA generated IMD are in multi-layer cellular network structures, where IMD from an MCPA-equipped micro-cell interfers with a macro-cell connected mobile [17], or as was investigated in [18], the mutual interference between an AMPS system BS using MCPA:s and a CDMA system mobile.

This paper shows how the use of multibeam antennas reduces the downlink IMD for the mobiles in the system. The radiation pattern provided by the beam-forming network will generate IMD that, in general, are radiated in directions different from the principal beam directions [19],[20],[21]. These IMD lobes have also been called "phantom lobes" [22] as they are not generated purposely, but is created by the nonlinearity. In effect, the array antenna spatially filters the IMP and this effect can in some circumstances be used to reduce the signal to intermodulation ratio of the mobiles in the system, as shown in [13] for a satellite system. The required circumstances to achieve this will be investigated in this paper. Furthermore, the spatially filtering of IMP:s can be utilized by the frequency channel allocation algorithm in the BS that assigns new mobiles to one of the empty frequency channels in the particular cell sector. If a non-frequency hopping system is assumed, each new mobile can be allocated to the frequency channel that generates least IMD to other mobile users in the same sector. This was briefly mentioned by Sandrin [19], and here an algorithm for this allocation procedure is proposed, and the performance is compared to a random frequency channel allocation algorithm. The solution is related to the recently proposed techniques for reducing IMD in a conventional one-antenna BS [23],[24] by spacing the used frequency channel unequally, to make the IMP fall onto unused frequency channels in between.

The remainder of this paper is organized as follows. Section 2 provides a description of the system model adopted. The switched multibeam array is defined as well as the nonlinear amplifier model. The beam-frequency scheme is defined in Section 3 and an algorithm for reducing the IMP by smart frequency channel allocation is presented and analyzed. Section 4 illustrates the IMD reduction with a numerical simulation of a GSM system with a multibeam BS while conclusions are drawn in Section 5.

2 System Model

The signal model for a cellular system using FDMA is defined in this section and beamforming using the FFT method is described. The MCPA is modeled using Cann's model for the amplifier and the method of Shimbo [25] is used to write the MCPA output signal in a comprehensive way. By deriving the far field signal from the array antenna in a specified direction Θ, it is shown how the transmitted signal can be described by a frequency-beam scheme, for use in the next section.

2.1 Signal Model

Assume a BS that provides service in one sector in a tri-sector cellular communication system. An N element uniformly spaced linear antenna array is used for reception and transmission of data to the users, although the study here considers the downlink transmission only. Furthermore, assume that M FDMA frequency channels are used in the particular sector, each with a bandwidth of W Hz and equally separated by Δ_ω, see Figure 2. Prior to, or integrated with each antenna, is an MCPA. It provides the signals with necessary gain to overcome the path loss and the fading in the radio channel. The signal that enters MCPA n (at antenna n) can be written in the form, [26]:

$$x_n(t) = \sum_{m=1}^{M} \sqrt{P_m} s_m(t) w_n \cos\left[(\omega_c + \omega_m)\, t + \phi_m(t) + \theta_{mn}\right] \tag{1}$$

where ω_c is the RF channel frequency reference and ω_m is the m:th sub-carrier frequency offset from this reference where $\omega_c \gg |\omega_m|$. Assume that the subcarrier's center frequencies, ω_m are equally spaced,

$$\omega_m = (m-1)\Delta_\omega + \omega_1 \quad . \tag{2}$$

Furthermore, $s_m(t)$ is the m:th sub-carrier envelope, after modulation and pulse shape filtering, P_m is the corresponding scaling to set the correct average transmitted power for sub-carrier m and $\phi_m(t)$ is the m:th sub-carrier phase. The transmitted information is contained in $\phi_m(t)$ for the phase modulation of the signal and in $s_m(t)$ for the amplitude modulation. Furthermore, w_n is the real taper weight at antenna n and θ_{mn} is the phase of the beamforming weight for sub-carrier m and antenna n. Using complex baseband signal notation, we can express (1) as

$$x_n(t) = Re\left\{\tilde{x}_n(t) \cdot e^{j\omega_c t}\right\} \tag{3}$$

provided that the bandwidth W is much less than the carrier frequency ω_c. $\tilde{x}_n(t)$ is the complex envelope of $x_n(t)$ and is a low-pass baseband signal. The complex envelope can be written as

$$\tilde{x}_n(t) = \sum_{m=1}^{M} \sqrt{P_m} s_m(t) w_n \cdot e^{j(\omega_m t + \phi_m(t) + \theta_{mn})} \quad . \tag{4}$$

The rest of this paper will use the complex baseband representation of signals.

2.2 Switched Multibeam Antenna Array

For the downlink beamforming in FDD systems, where the downlink channel is unknown, one choice is to transmit in the direction where the largest average power from our particular user in the uplink was received. The low side-lobes of the radiation pattern decreases the co-channel interference to users in neighboring cells. A linear array antenna with N antenna elements can generate N beams with distinct spatial orientations in the horizontal plane, by use of a beam forming network (BFN). Assume further that the taper weighting w_n is unity, $w_n = 1, n = 1, \ldots, N$. Taper weighting can be used to reduce side-lobe levels at the expense of increased beam-width of the main-lobe and loss in antenna gain [27].

Furthermore, a FFT based BFN often implemented as a Butler matrix [28],[29] is assumed. It has the property of a constant phase gradient $\Delta\theta_m$ over the antenna array aperture, yielding

$$\theta_{nm} = (n-1)\Delta\theta_m \tag{5}$$

for $n = 1, \ldots, N$. The phase gradient, $\Delta\theta_m$ belongs to the set $\mathbf{\Omega_S}$ of N different phase gradients, unique for each beam the BFN can generate,

$$\Omega_S = \left\{ \frac{2\pi p}{N} \right\}_{p=0}^{N-1} \tag{6}$$

The finite set Ω_S is a closed group under multiplication and addition, following *modulo* N algebra. These properties implies that the main-lobe direction of the desired signals are also main-lobe directions for the IMD, as will be shown later.

2.3 Nonlinear Multicarrier Power Amplifier

To model the amplifier nonlinearity, the memoryless envelope limiter model, proposed by Cann [30] is used in the analysis. It is described by the baseband transfer characteristic

$$\tilde{y}(t) = \frac{Dsgn(\tilde{x}(t))}{\left[1 + \left(\frac{l}{|\tilde{x}(t)|}\right)^s\right]^{1/s}} = F(\tilde{x}(t)) \tag{7}$$

where $\tilde{y}(t)$ is the instantaneous output, $\tilde{x}(t)$ the instantaneous input, D the asymptotic output level as the input amplitude $|\tilde{x}(t)| \to \infty$, $sgn(\tilde{x}(t))$ the signum function, l the input limit level and s is the knee sharpness. Cann's model is used for its parametric form as opposed to polynomial amplifier models which are better suited when fitting experimental data to a model. In Cann's model the degree of linearity is easily adjusted by varying the parameter s.

To yield the bandpass nonlinearity corresponding to the baseband model, we use the Chebychev transform [31]

$$f_1(|\tilde{x}(t)|) = \frac{1}{\pi}\int_0^{2\pi} F\left(|\tilde{x}(t)|\cos\alpha\right)\cos\alpha d\alpha \tag{8}$$

and a similar integral is calculated as

$$f_2(|\tilde{x}(t)|) = \frac{1}{\pi}\int_0^{2\pi} F\left(|\tilde{x}(t)|\cos\alpha\right)\sin\alpha d\alpha \tag{9}$$

by necessity, often by using numerical methods. The function defined as $f(|\tilde{x}(t)|) = \sqrt{f_1(|\tilde{x}(t)|)^2 + f_2(|\tilde{x}(t)|)^2}$ is commonly denoted as the AM/AM conversion characteristic of the amplifier and $g(|\tilde{x}(t)|) = \tan^{-1}\{f_2(|\tilde{x}(t)|)/f_1(|\tilde{x}(t)$ as the AM/PM conversion characteristic. With these functions at hand[1], the analytic signal input/output relation for the MCPA at antenna n can now be written as

$$\tilde{y}_n(t) = f\left(|\tilde{x}_n(t)|\right)\exp\left[j\phi_{x_n}(t) + jg(|\tilde{x}_n(t)|)\right] \tag{10}$$

where $\phi_{x_n}(t)$ is the phase of the input signal $\tilde{x}_n(t)$.

Now, define the amplifier saturated output power P_o^{sat} as the maximum RF power supplied by the amplifier when driven by a CW signal having power P_i^{sat}. The input back-off (IBO) can now be defined as $IBO = P_i^{sat} - P_{in}$ in decibels, where P_{in} is the average input power. As the input signal is a multicarrier signal, the average input power is estimated in the simulations during a pre-run phase and then the negative gain in decibels to set the correct IBO for the amplifier is introduced.

2.4 Combining MCPA performance with Spatial Description

The multicarrier input signal (4), to the MCPA generates a large number of intermodulation products (IMP) in the output signal, and a combinatorial problem follows to determine the frequency and relative phase of each of the IMP:s. Adding the complexity of an array antenna, the spatial dispersion of the IMP:s must also be considered. To calculate the direction of each of these IMP:s a rewriting of equation (10) is used for the output of MCPA n as

$$\tilde{y}_n(t) = \sum_K S\left[K; A_1(t), A_2(t), \cdots, A_M(t)\right]\exp\left(j\sum_{m=1}^{M} k_m\left(\omega_m t + \phi_m(t) + \theta_{mn}\right)\right) \tag{11}$$

where K is the following set of integer indices

$$K = \left\{\{k_1, k_2, \ldots, k_M\} : \sum_{m=1}^{M} k_m\omega_m = \omega_p\right\} \tag{12}$$

to consider the output in the frequency channel with center frequency ω_p only. If ω_p is one of the sub-carriers center frequencies $(\omega_1, \ldots, \omega_M)$, the summation in (11) will be restricted to terms that lie in the

[1]Laboratory measurements of nonlinear amplifiers give the $g(|\tilde{x}(t)|)$ and $f(|\tilde{x}(t)|)$ functions directly, so by working with measured amplifier characteristics, the integrals (8),(9) need not be evaluated

zone of the first harmonic (fundamental) of the output signal. To study the fundamental and third order IMP solely, K in (11) is easily exchanged for the subset $K_{1,3}$, defined as

$$K_{1,3} = K \cap \left\{ \{k_1, k_2, \ldots, k_M\} : \sum_{m=1}^{M} |k_m| = 1, 3 \right\} \quad . \tag{13}$$

Furthermore, in equation (11), $A_m(t) = \sqrt{P_m} s_m(t)$ is the sub-carrier m:s envelope, where unity taper weights w_n has been assumed. The complex valued function $S[\cdot]$ is known as the Shimbo amplitude function (SAF)[25][32], and gives the amplitude and relative phases of the output intermodulation products with indices $\{k_i\}_{i=1}^{M}$. The calculation of SAF involves the amplifier characteristics $f(\cdot)$, $g(\cdot)$ and the envelope of the sub-carriers in the multicarrier input signal. The explicit values of the SAF:s are not required in the following analysis. If the amplifier does not exhibit any AM/PM conversion, the SAF will be real. Note that SAF depends on the envelopes and not the phases of the input sub-carrier signals.

2.5 The far field radiation pattern

As a tri-sector system was assumed, the interval $-\pi/3 < \Theta < \pi/3$ is of interest, where the angle Θ is measured from broadside of the array. The complex envelope of the received signal $z(t, \Theta)$ at a hypothetical user in direction Θ is represented by a discrete complex sequence $z(l, \Theta)$ of L samples [33].

$$z\left(l, \Theta\right) = \gamma(\Theta) \sum_{n=1}^{N} \tilde{y}_n(l) e^{-jd\omega_c(n-1)\sin(\Theta)/c} \tag{14}$$

where $l = 0, \ldots, L-1$, d is the array inter-element spacing, c the speed of light and $\gamma(\Theta)$ is the individual antenna element gain in direction Θ which is assumed equal for all N antenna elements. The far field effective isotropic radiated power (EIRP) in direction Θ from broadside direction is defined as

$$P_{EIRP}(\Theta) = \left| \frac{z(l, \Theta)}{N} \right|^2 = \left| \frac{\gamma(\Theta)}{N} \sum_{n=1}^{N} \tilde{y}_n(l) e^{-jd\omega_c(n-1)\sin(\Theta)/c} \right|^2 \quad . \tag{15}$$

By inserting (11) into equation (15) one finds that for a particular set of indices, $\{k_i\}_{i=1}^{M}$, which uniquely labels any IMP, and by using (5) for the FFT based BFN, an equivalent phase gradient for the particular IMP is calculated as

$$\Delta\theta_{eq} = \sum_{m=1}^{M} k_m \Delta\theta_m \tag{16}$$

which will maximize the P_{EIRP} in a direction given by the angle

$$\Theta = \sin^{-1}\left(\frac{c\Delta\theta_{eq}}{d\omega_c} \right) \quad . \tag{17}$$

Hence, two signals, say $\tilde{x}_1(t)$ and $\tilde{x}_2(t)$, separated according to (2), with equal phase gradients ($\Delta\theta_1 = \Delta\theta_2$), will generate third order IMP with equal phase gradients $\Delta\theta_{eq} = \Delta\theta_1 = \Delta\theta_2$, i.e. IMP at the frequencies $\omega_3 = 2\omega_2 - \omega_1$ and $\omega_0 = 2\omega_1 - \omega_2$ are radiated in the same beam directions as the amplified original signals $\tilde{x}_1(t)$ and $\tilde{x}_2(t)$. If, however the two signals are to be transmitted in distinct beams, $\Delta\theta_1 \neq \Delta\theta_2$ and the third order IMP are radiated with phase gradients $2\Delta\theta_2 - \Delta\theta_1$ and $2\Delta\theta_1 - \Delta\theta_2$ at the frequencies $\omega_3 = 2\omega_2 - \omega_1$ and $\omega_0 = 2\omega_1 - \omega_2$ respectively. Note that ω_0 is outside the defined transmitter band, and can be removed by the transmit filter.

3 Utilizing the Combined Beam-Frequency Scheme

It is possible to systematically calculate the *beam-frequency slot* where the main beam of an IMP appears. In this section, we show how this can be used to reduce the IMD power radiated towards the mobiles in the system.

3.1 The number of IM products

Given M active, co-amplified sub-carriers on equally spaced frequency channels in the MCPA, the number of generated IMP in the output signal is required to calculate the IMD in the system. The following analysis is restricted to third order IMP. Type A IMP is defined as the cross-modulation term $2\omega_i - \omega_j$ and type B IMP as the composite triple-beat terms $\omega_i + \omega_j - \omega_k$. Type B IMP becomes more deleterious when the total bandwidth is less than an octave because most of the type A IMP falls fall outside the band of interest [23]. The center frequency channel is the worst channel among all the channels, because the largest number of third-order IMP terms ν_c, [23]:

$$\nu_c = \frac{3}{8}\left(M^2 - 2M + 1\right) \tag{18}$$

falls onto the center channel. The ν_c IMP in the center channel can be divided into M_A type A as [24]

$$\begin{array}{ll} M_A = (q-1) & \text{if } M\text{=2q} \\ M_A = 2\lfloor q/2 \rfloor & \text{if } M\text{=2q+1} \end{array} \tag{19}$$

and the number of type B IMP, $M_B = \nu_c - M_A$. Furthermore, assume that the center channel is left empty, as common in noise power ratio (NPR) measurements, all IMP involving the carrier in the center channel most be subtracted from (18). This gives, after some calculations

$$\nu_c^e = \frac{1}{8}\left(3M^2 - 10M + 7\right) \tag{20}$$

where it is assumed that M is an odd number.

3.2 Beam-frequency scheme

Using the above definitions, given a set of M equally spaced frequency channels, and a set of N beams, the beam-frequency scheme can be defined, which can be used to reduce the IMP levels in the system. Main beam IMP is defined as the direction of the maximum radiation intensity of the particular IMP. Certainly, IMP will be radiated in all directions, but suppressed by the side-lobe of the array radiation pattern in other directions than the main beam direction. A slot is defined as a beam-frequency pair consisting of a frequency channel and a main beam direction generated by the BFN. IMP that comes from adjacent cells are neglected, as the (linearly amplified) co-channel interference from adjacent cells are a more severe source of interference than the (non-linearly amplified) IMD from adjacent cells.

Furthermore, the FFT based BFN is used, so the properties of closeness and finiteness of the *modulo* N addition and multiplication of the phase gradients (16) makes the main beam direction of the IMP coincide with the set of main beam directions for the desired (linearly amplified) signals. Fig. 3 shows an example of the beam-frequency scheme where three users have been randomly assigned (in frequency) to three slots. The figure shows the slots where main beams of type A and type B IMP will appear (type B IMP312, and two type A IMP23, IMP21). The N=4 element antenna array will certainly reduce the amount of IM distortion at the mobile as compared to the reference N=1 antenna BS in Fig. 3(b) because main beam IMP falls onto other beam slots, or stated differently, in other directions than the user main beams. Hence, the IMP will be suppressed by the side-lobes of the antenna array radiation pattern.

3.3 Reducing the IMD by using an antenna array

To calculate the reduction in IMD due to the use of a multibeam antenna, statistical methods must be used, as the activity of the users as well as their angle Θ seen from the BS, are stochastic processes. In the analysis, a fully loaded system (all M frequency channels occupied), is assumed where M is an odd number. The center channel is chosen for the analysis, i.e. frequency channel q where $M = 2q + 1$. Assume further that the angle position of the active mobiles are independent and uniformly distributed in the range $[-\pi/3, \pi/3]$. If the N beams have equal beam-width, the probability that a user is active in a specific beam is $1/N$. The number of IMP of type A or type B falling on any particular beam-frequency

slot n then becomes binomially distributed $Bin(M_x,1/N)$ as

$$P_{M_x}(\nu) = \left(\begin{array}{c} M_x \\ \nu \end{array} \right) \left(\frac{1}{N}\right)^{\nu} \left(1 - \frac{1}{N}\right)^{M_x - \nu} \tag{21}$$

where $x = A, B$.

The expectation value of (21) is M_A/N and M_B/N for type A and B IMP respectively and the variance is $M_A(N-1)/N^2$ and $M_B(N-1)/N^2$ respectively. If the number of IMP in a specific beam slot is less than the mean value of (21), the IMD power in this direction is less than average. If the number of frequency channels M is increased, and keeping the number of beam directions N fixed, the quotient of the number of IMP in a beam compared to the $N-1$ other beams is on average approaching unity. By defining the normalized variance, or *variability*, υ, of the distribution (21), as

$$\upsilon = \frac{N-1}{M_x} \tag{22}$$

for $x = A, B$, it is possible to study this. The variability indicates that when the number of IMP of type x, M_x, is increased, as when the number of frequency channels M is increased, the IMP are evenly distributed over all beams, and the total IMP radiation pattern, which is the sum of all IMPs, is approaching the radiation pattern of a single antenna element. Note that the individual IMP maintain their ideal array pattern, but their sum has a "smoothing" effect on the radiated IM power. This was also observed in [14]. By increasing the number of antennas N, the variability (22) is increased, and the total IMP radiation pattern directivity is increased, i.e. lobes are formed is some directions. For higher order IMPs, the number of IMPs, M_x, is a large number compared to N and the small variability leads to a radiation pattern close to the single antenna element pattern.

Hence, it is expected that by using a N beam array antenna, the IM power experienced by the users, compared to a reference $N = 1$ conventional BS, are on average reduced $10\log_{10}(N)$ dB, as the number of main beam IMP towards the mobile are on average reduced by the factor $1/N$. Note that the transmitted power from each antenna is reduced by $20\log_{10}(N)$ dB compared to the N=1 antenna case, to yield the same received power at the mobile.

If the number of active frequency channels is less than M, which is the normal case[2], it is shown below how it is possible to reduce the amount of IMD further, by utilizing the extra degree of freedom the N beams provide.

3.4 IM-reducing frequency channel allocation

Assume a non-frequency hopping system, or a system with deterministic frequency hopping in the following. In the example of Fig.3, a new user can be placed in any of the empty frequency channels $F2$,$F4$ or $F6$. Depending of the beam allocation for the new user (which is out of the basestations control, it depends on the spatial position of the new user), the basestation should allocate the new user to a frequency channel that produces the lowest number of "collisions", where a collision has taken place when the generated main beam IMP falls into a slot that is occupied by a user. The basestation performs a search over all free slots and calculates the number of collisions in the $M \times N$ beam-frequency scheme for each case. When a call is dropped, a new frequency channel is available and added to the set of searched slots for the next new user.

To compare the proposed algorithm, the expected value of the number of collisions is calculated and compared with a random frequency channel allocation algorithm. The number of slot collisions depends on the number of available beams and on the number of active users in the particular sector. Define the probability p_{ch} as the probability that a given frequency channel is in use in a cell, which is a function of the offered traffic A_o (in Erlang), the blocking probability P_B and the number of frequency channels M in the sector [3],

$$p_{ch} = \frac{A_o}{M}(1 - P_B) \tag{23}$$

[2]M active frequency channels corresponds to a blocking probability of one for a new user, and is a rare case if the system capacity is properly planned.

The number of active users in the sector is a random variable varying from zero to M and has binomially distribution $P_a(m) \sim Bin(M, p_{ch})$ [3]. If blocked calls are cleared (calls arriving when all the channels are found to be busy are lost), the blocking probability is given by the Erlang-B formula

$$P_B = \frac{A_o^M / M!}{\sum_{k=0}^{M} A_o^k / k!} \quad . \tag{24}$$

To derive the expected number of collisions C, the conditional expectation

$$E\{C\} = \sum_{m=0}^{M} E\{C|m\} P_a(m) \tag{25}$$

is used, where E is the expectation operator. The conditional expectation value $E\{C|m\}$ of C collisions conditioned on m active users involves summation over all possible beam-frequency slot allocations and its calculation is a formidable task. It depends on the chosen frequency channel allocation algorithm, the number of beams N, the number of frequency channels M and on the blocking probability P_B. To illustrate how the algorithms performs, an example is presented, where a Monte Carlo simulation method is used to estimate $E\{C|m\}$ and calculate the expectation of C.

The system is simulated with M=9 frequency channels and blocking probability $P_B = 2\%$. This gives, by using (24) the offered traffic A_o=4.34 Erlang per sector and hence a channel activity p_{ch} of 47.3%. The simulation is performed as follows. In each simulation step, a mobile is activated in a random direction or a random mobile drops its call. This is simulated by using a generalized birth-death process with $M + 1$ states [34]. For each new mobile, all unoccupied frequency channels are searched and the number of collisions are counted. The slot allocation that gives the fewest collisions is chosen for the new user. If two or more slots give the same number of collisions, the total number of generated IMP in the $N \times M$ beam-frequency scheme is calculated for the slots that gave the same number of collisions, and the algorithm choose the slot that generates the fewest IMP. 10 000 steps were performed to estimate $E\{C|m\}$ for each case of N=8,4,2 and also N=1 for comparison. Table 1 shows the reduction in number of collisions when the proposed algorithm is used as compared to random frequency channel allocation. It is interesting to see that four beams and using the proposed algorithm, has on average fewer collisions than an eight beam system using a random frequency channel allocation. This can also be seen in Fig. 4 where random/N=8 have a higher collision count than the best/N=4 algorithm, when the number of active users are less than seven.

When the number of beams (antennas) is increased, the beam-width of the main beam is narrower and hence, the IMP is concentrated into narrower beams. Hence, it is less likely that a user collides with the main beam of an IMP, and as seen in Table 1, the number of collisions is reduced.

4 Computer Generated Results

Due to the random positions of the users, and also the stochastic nature of the number of active users, the IMD power as experienced by a mobile user in the system will be a random variable. Hence, to study the improvement in carrier to intermodulation ratio by using a multibeam antenna, as discussed in the previous sections, the probability distribution function (PDF) of the IMD power at the mobile is estimated using simulations. We assume a channel separation and modulation that resemble the GSM system. The variation of the shape and position of the PDF with the parameters N and M are discussed and conclusions is drawn.

A common method to measure the effect of nonlinearities in multicarrier communication systems, is to use a measurement channel, centered in the frequency channel plan. This unoccupied center channel will, on the MCPA output contain IMP, and the effect of distorting the input signal can directly be related to the output power in the unoccupied channel [35].

4.1 Modulation and Sampling Rates

Assume that each sub-carrier is GMSK modulated with a bit rate T_b=271 kbit/s, together with a Gaussian low pass pulse-shaping filter with a normalized bandwidth BT_b=0.3 and filter length of six bits. A

minimum sampling frequency of 50 samples per symbol is used in the simulations for the sub-carrier with largest ω_m to ensure an accurate representation of the generated intermodulation distortion. Using M=9 channels, this yields a multichannel sampling rate of 67.75 MHz. The length of a data burst is 156 bits and consists of randomly generated data for each user.

4.2 Adjacent Channel Distortion Simulation

To measure the distortion introduced by the nonlinearities in the MCPA and the effect of beamforming for the spatial distribution of this distortion, a simulation, illustrated in schematic form in Fig.5 is performed. The method measures the interference in an unoccupied channel placed in the center of the transmitted frequency band. Hence, the input frequency channels centered at $\omega_1, \omega_2, \ldots, \omega_{e-1}, \omega_{e+1}, \ldots, \omega_M$ are occupied, while the center channel at ω_e is unoccupied. This center channel will receive intermodulation distortion and sideband regrowth from the modulated channels.

Since most communication systems are designed to meet a certain level of adjacent channel interference, the output power in this unoccupied channel can directly be related to the performance of the system. Note that the center channel contains contributions from all other channels and the power measured there is therefore the worst possible case of interference. The channel spacing Δ_ω is set to $3W$ to assure that the spectral truncation noise, due to finite impulse response filtering, of the channels immediately below and above the unoccupied channel does not increase the spectral content in the unoccupied channel.

The $L = 156 \times 50 \times 5 = 39000$ samples of the received signal in direction Θ is collected and a Hanning window function is applied before the discrete Fourier transform (DFT) is calculated. The signal is filtered in an ideal 30 kHz bandpass filter centered at ω_e and the power level in the unoccupied channel is measured (this is equivalent to the procedure described in the GSM 05.05 specification [35]). The intermodulation power is obtained using power spectrum analysis, define the Hanning windowed DFT of $z(l, \Theta)$ as [36]:

$$Z(p, \Theta) = \sum_{l=0}^{L-1} z(l, \Theta) w_H(l) e^{j2\pi p(l/L)} \tag{26}$$

for $p = 0, \ldots, L-1$ and $w_H(l)$ is the Hanning window function. The power in the measurement bandwidth in direction Θ can now be written as

$$P_r(\Theta) = 10 \cdot \log_{10} \left[\frac{1}{p_2 - p_1 + 1} \sum_{p=p_1}^{p_2} |Z(p, \Theta)|^2 \right] \tag{27}$$

and p_1, p_2 are chosen to obtained an ideal bandpass filter of 30 kHz bandwidth, centered at ω_e.

Cann's model, (7) was used to model the power amplifier with parameters $s = 8$, $D = 1$, $l = 1$ and the IBO was set to 10 dB, regardless of M, as described in Section 2.3. Fig. 6 shows an example of the radiation pattern (27) in the empty frequency channel, centered at ω_e and normalized to a common reference so the maximum power in the $M = 8, N = 4$ case is 0 dB. With the number of active carriers M=8, a higher level of IM interference is measured, compared to when M=4, as expected. The number of third-order IMP terms can be calculated by (20) to $\nu_c^e = 20$ and 4 for the $M = 8$ and $M = 4$ case respectively[3]. When the variability υ in (22) is decreased, the IMP radiation pattern gets smoothed and approaches the single element pattern. This is visible in the $N = 4$, $M = 8$ case in Fig. 6.

If the received power at the test mobile when using $N = 1$ antennas at the basestation is used as a reference, the PDF of the difference (in dB) between the $N = 1$ and $N > 1$ case for a particular set of mobile locations is estimated using 200 data bursts. Random frequency allocation is performed and no power control is used. See Fig. 7 and 8 for the $M = 5$ and $M = 9$ case respectively (where the measurement is made in the empty center channel, as before). Note that the IBO is equal for the different antenna configurations, hence an increase in number of antennas, leads to a reduced output power of each MCPA, but the IBO is kept equal in the simulations, to allow an analysis of the spatial dispersion effect of the IMP only. Table 2 shows the mean of the PDFs in Fig. 7 and Fig. 8. According to the discussion in section 3, a reduction in the IM power of $10 \log_{10}(N)$ dB is expected. For the M=9 case, the number of IMP is so large that approximately $1/N$ of them reach the mobile at maximum power, that is, in the main-lobe of the array antenna radiation pattern. However, the $M = 5$ case allows larger

[3]Note that M=9 and M=5 is used in (20), but the center channel is left empty

variations in the distribution of the IMPs over the N beams, i.e. a larger variability, and a deviation from the $10\log_{10}(N)$ expression is increased. Note that in the $N = 8, M = 5$ case, the probability that a mobile is not in the direction of an IMP main beam in the empty center frequency channel is from (21), $P_\nu(0) = \left(\frac{8-1}{8}\right)^{\nu_c^e}$=0.59 where ν_c^e=4 is the total number of IMP in the center channel given by (20). This explains the relatively high probability for a very large reduction (5-20 dB) in IMP power for $N = 8$ in Fig. 7, as compared to the $N = 2$ case in the same figure, where $P_\nu(0)$=0.0625.

The $M = 9$ case in Fig. 8 shows the case of a large number of third order IMP. As the number of beams N is increased, the mean of the IMP is decreased but the width of the PDF increases (increased variability), due to larger variations in the number of IMP per beam. Furthermore, the probability that a mobile receives no main beam IMP $P_\nu(0)$ is in this case very small.

5 Conclusions

The effect of a nonlinear transmit amplifiers in a switched beam base-station antenna for a cellular system using FDMA has been analyzed. It has been found that the main beam direction of the IMP is in general different from the directions of the principal signal beam directions. It was shown how the increased number of degrees of freedom when introducing an array could be utilized to reduce the received IMD at the mobile users. This is achieved by assigning new users to frequency channels that minimizes the IMD at other mobile users in the same sector, hence the IMP are "placed" in directions were no mobile user exists on that frequency. The proposed algorithm outperforms a random channel allocation method and the improvement is increasing with the traffic load and the number of antenna elements.

To study the expected value of the IMD reduction at the mobiles, a Monte Carlo simulation was used to estimate the PDF of the mobile CIR for an example GSM system. With increased number of antenna elements and a low number of active channels, the IMD reduction as compared to the N=1 reference antenna case has a larger dynamic range. In this case, it is possible, especially if a smart frequency allocation strategy is used, that the mobile user experiences no main beam IMD, hence a large IMD reduction compared to the reference case is gained. It was also shown that when the number of active users is larger than the number of available beams, the width of the PDF is smaller and $10\log_{10}(N)$ dB reduction in IMD is the most likely improvement.

References

[1] S.Andersson, B.Carlqvist, B.Hagerman, and R.Lagerholm, "Enhancing cellular network capacity with adaptive antennas," *Ericsson Review*, vol. 76, pp. 138–141, 1999.

[2] D.Shim and S.Choi, "Should the smart antenna be a tracking beam array or switching beam array?," in *Proceedings of Vehicular Technology Conference*, Ottawa, Canada, 1998, pp. 494–498.

[3] S.S. Swales, M.A. Beach, D.J. Edwards, and J.P. McGeehan, "The performance enhancement of multibeam adaptive base-station antennas for cellular land mobile radio systems," *IEEE Transactions on Vehicular Technology*, vol. 39, pp. 56–67, 1990.

[4] H.Dam, M.Berg, S.Andersson, R.Bormann, M.Frerich, and T.Henβ, "Performance evaluation of adaptive antenna base stations in a commercial GSM network," in *Proceedings of Vehicular Technology Conference*, Piscataway, USA, 1999, pp. 47–51.

[5] S.Andersson et.al., "Ericsson/Mannesmann GSM field trials with adaptive antennas," in *Proceedings of Vehicular Technology Conference*, Phoenix,USA, 1997, pp. 1587–1591.

[6] C.R.Ward, D.N.Adams, F.M.Wilson, K.S.Wilson, and A.K.Bush, "The live-air trial of a multi-beam cellular base station antenna system," in *IEE National Conference on Antennas and Propagation*, London, UK, 1999, pp. 169–172.

[7] S.Andersson and B.Hagerman, "Adaptive antennas in wireless systems-basic background and field-trial results," in *Proceedings of Radiovetenskaplig Konferens*, Karlskrona, Sweden, 1999.

[8] M.J.Ho, G.L.Stuber, and M.D.Austin, "Performance of switched-beam smart antennas for cellular radio systems," *IEEE Transactions on Vehicular Technology*, vol. 47, pp. 10–19, 1998.

[9] P.Petrus, R.B.Ertel, and J.H.Reed, "Capacity enhancement using adaptive arrays in an AMPS system," *IEEE Transactions on Vehicular Technology*, vol. 47, pp. 717–727, 1998.

[10] K.I. Pedersen, P.E. Mogensen, and F.Fredriksen, "Joint directional properties of uplink and downlink channel in mobile communication," *Electronic Letters*, vol. 35, pp. 1311–1312, 1999.

[11] G.Tsoulos, M.Beach, and J.McGeehan, "Space division multiple acess (SDMA) field trials. Part 2: Calibration and linearity issues," *IEE Proc. - Radar, Sonar and Navigation*, vol. 145, pp. 79–84, 1998.

[12] K.J. Maalouf, R.C.Gaus, and S.Sowelam, "Error rate estimation in a multi-channel active phased array," in *IEEE International Conference on Communications*, New York, USA, 1998, pp. 402–406.

[13] P.A. Chiavacci, "Analysis of noise power ratio effects on satellite communication system performance," *Microwave Journal*, vol. 40, no. 6, pp. 24–34, 1997.

[14] R. De Gaudenzi, "Payload nonlinearity impact on the globalstar forward link multiplex part I: Physical layer analysis," *IEEE Transactions on Vehicular Technology*, vol. 48, pp. 960–976, 1999.

[15] H. Xue, R. Davies, M.Beach, and J. McGeehan, "Linearity considerations in adaptive antenna array applications," in *Proceedings of the Sixth International Symposium on Personal, Indoor and Mobile Radio Communications*, Toronto, Canada, 27-29 September 1995, pp. 682–686.

[16] 3rd Generation Partnership Project; Technical Specification Group Radio Access Networks, "TS 25.141 base station conformance testing (FDD) (Release 1999)," 2000.

[17] J.Shi and K.Arvidsson, "Performance of multi-carrier power amplifiers in hierarchical cell structure," in *Proceedings of Vehicular Technology Conference*, Ottawa, Canada, 1998, pp. 1622–1625.

[18] K.Hamied and G.Labedz, "AMPS cell transmitter interference to CDMA mobile receiver," in *Proceedings of Vehicular Technology Conference*, New York, USA, 1996, pp. 1467–1471.

[19] W.A. Sandrin, "Spatial distribution of intermodulation products in active phased array antennas," *IEEE Transactions on Antennas and Propagation*, vol. 22, pp. 864–868, 1973.

[20] S.L.Loyka, "The influence of electromagnetic environment on operation of active array antennas: analysis and simulation techniques," *Antennas and Propagation Magazine*, vol. 41, pp. 23–39, 1999.

[21] M.Wennström, "Considering downlink intermodulation distortion in switched multibeam antennas for cellular radio systems," in *Proceedings of Vehicular Technology Conference*, Boston, USA, 2000, pp. 1858–1865.

[22] J.Litva and T.Lo, *Digital beamforming in wireless communications*, Artech-house Publishers, Boston, 1996.

[23] H.Jung and O.K.Tonguz, "Random spacing channel assignment to reduce the nonlinear intermodulation distortion in cellular mobile communications," *IEEE Transactions on Vehicular Technology*, vol. 48, pp. 1666–1675, 1999.

[24] B.Hwang and O.K.Tonguz, "A generalized suboptimum unequally spaced channel allocation technique-part I:In IM/DD WDM systems," *IEEE Transactions on Communications*, vol. 46, pp. 1027–1037, 1998.

[25] O.Shimbo, "Effects of intermodulation, AM-PM conversion, and additive noise in multicarrier TWT systems," *Proceedings of the IEEE*, vol. 59, no. 2, pp. 230–239, 1971.

[26] M.Wennström, "Smart antenna implementation issues for wireless communications," Tech. Rep., Signals and Systems Group, Uppsala University, Sweden, 1999, Technical Licentiate Thesis, http://www.signal.uu.se/Publications/ abstracts/l991.html.

[27] Merril I. Skolnik, *Introduction to Radar Systems*, McGraw Hill, Auckland, 1980.

[28] J.L. Butler, *Digital matrix and intermediate frequency scanning, Scanning Antennas*, vol. 3, Academic Press, 1966.

[29] J.P Shelton and K.S. Kelleher, "Multiple beams from linear arrays," *IRE Transactions on antennas and propagation*, vol. 9, pp. 154–161, 1961.

[30] A.J.Cann, "Nonlinearity model with variable knee sharpness," *IEEE Trans. on Aerospace and Electronic Systems*, vol. 16, pp. 874–878, 1980.

[31] M.C. Jeruchim, *Simulation of communication systems*, Plenum Press, New York, New York, 1992.

[32] K.W. Schneider and W.H.Tranter, "Efficient simulation of multicarrier digital communication systems in nonlinear channel environments," *IEEE Journal on selected areas in communications*, vol. 11, no. 3, pp. 328–339, 1993.

[33] C. Balanis, *Antenna Theory, Analysis and Design*, John Wiley and Sons, New York, 1982.

[34] M.D. Yacoub, *Foundations of Mobile Radio Engineering*, CRC Press, Boca Raton, Florida, 1993.

[35] D.W.Bennett, P.B.Kenington, and R.J.Wilkinson, "Distortion effects of multicarrier envelope limiting," *IEE Proceedings on Communications*, vol. 144, no. 5, pp. 349–356, 1997.

[36] M. Hayes, *Statistical digital signal processing and modeling*, John Wiley and Sons, Inc, New York, 1996.

List of Figures

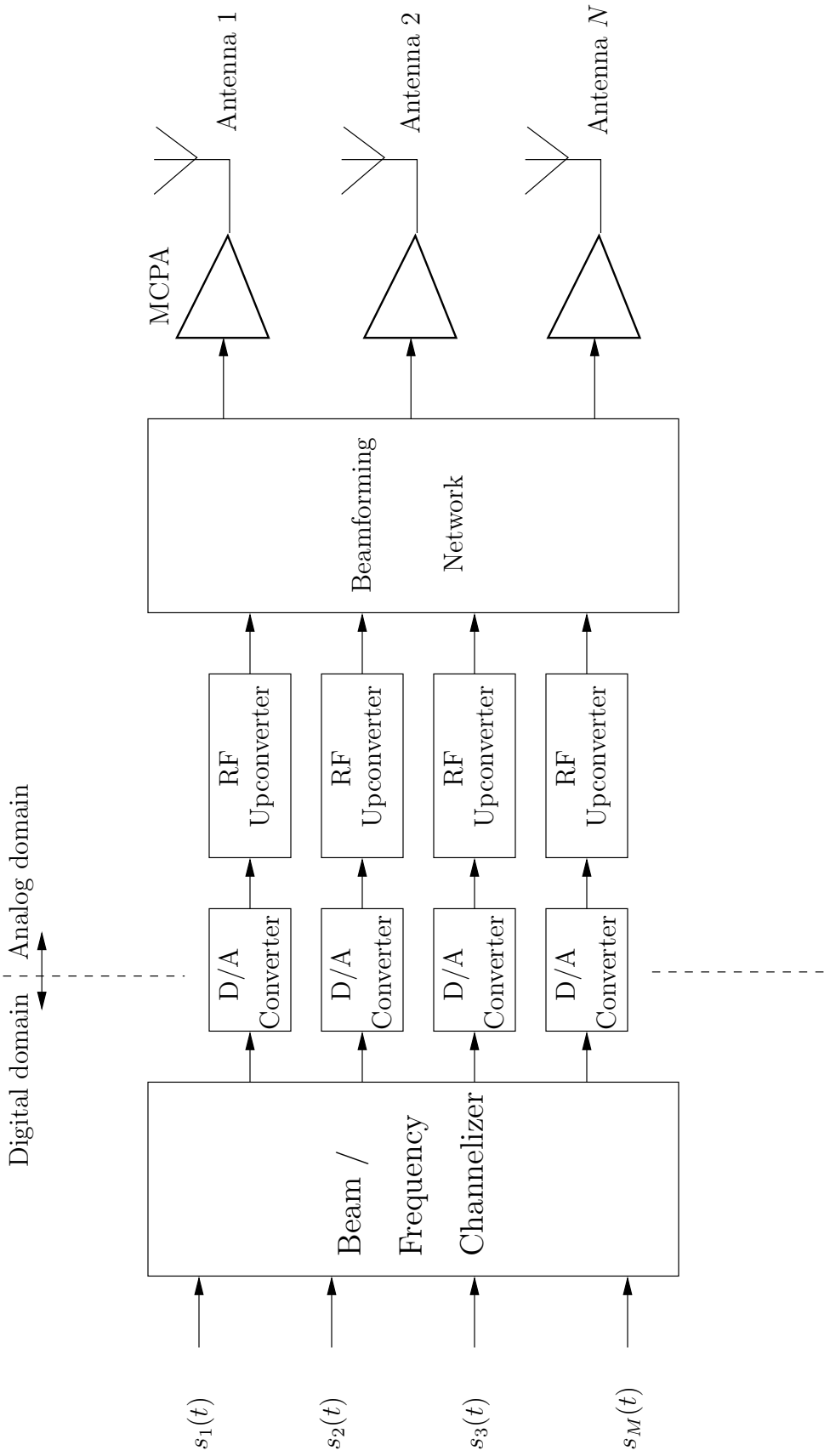

Figure 1: Switched multibeam array architecture. The beam/frequency channelizer directs the input signals to their respective FDMA frequency slots and weights picks the "best" downlink beam using uplink information.

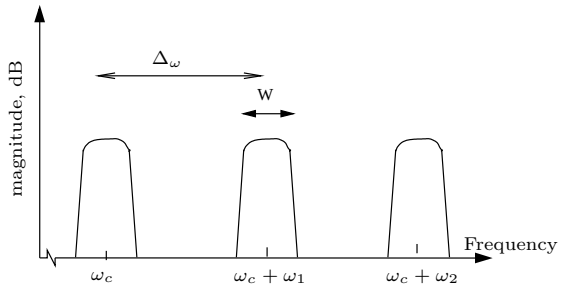

Figure 2: Input signal spectrum to the multicarrier amplifier. The sub-carriers of width W Hz are separated Δ_ω Hz.

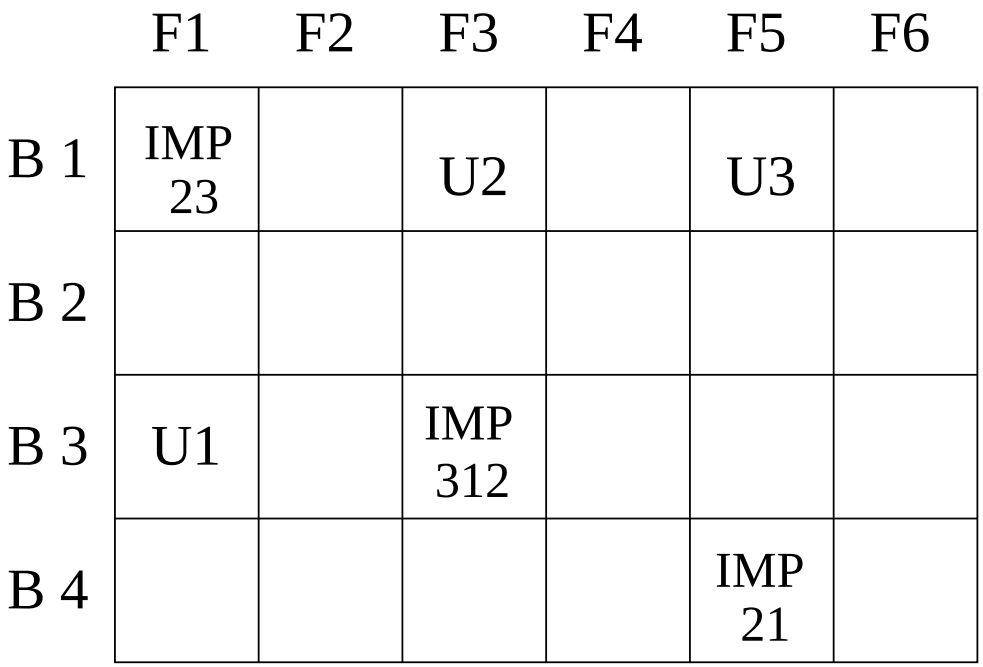

(a)

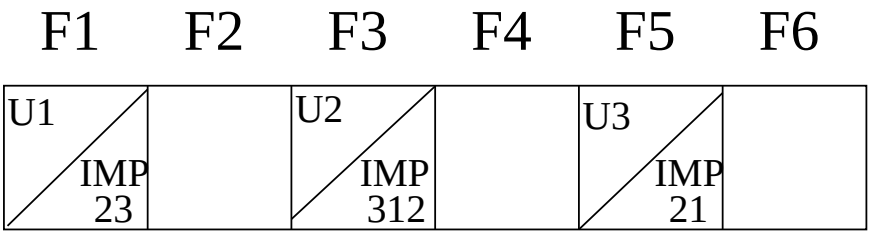

(b)

Figure 3: Beam-frequency scheme for (a) N=4, (b) N=1, where M=6. The figure shows three active users (U1,U2,U3) occupying three FDMA slots. Only third order IMP that falls in the frequency channels of interest ($F1$-$F6$) are considered. Type A IMP is denoted "IMP ab" when user a and b generates the IMP. User 1,2,3 generates type B IMP denoted "IMP abc".

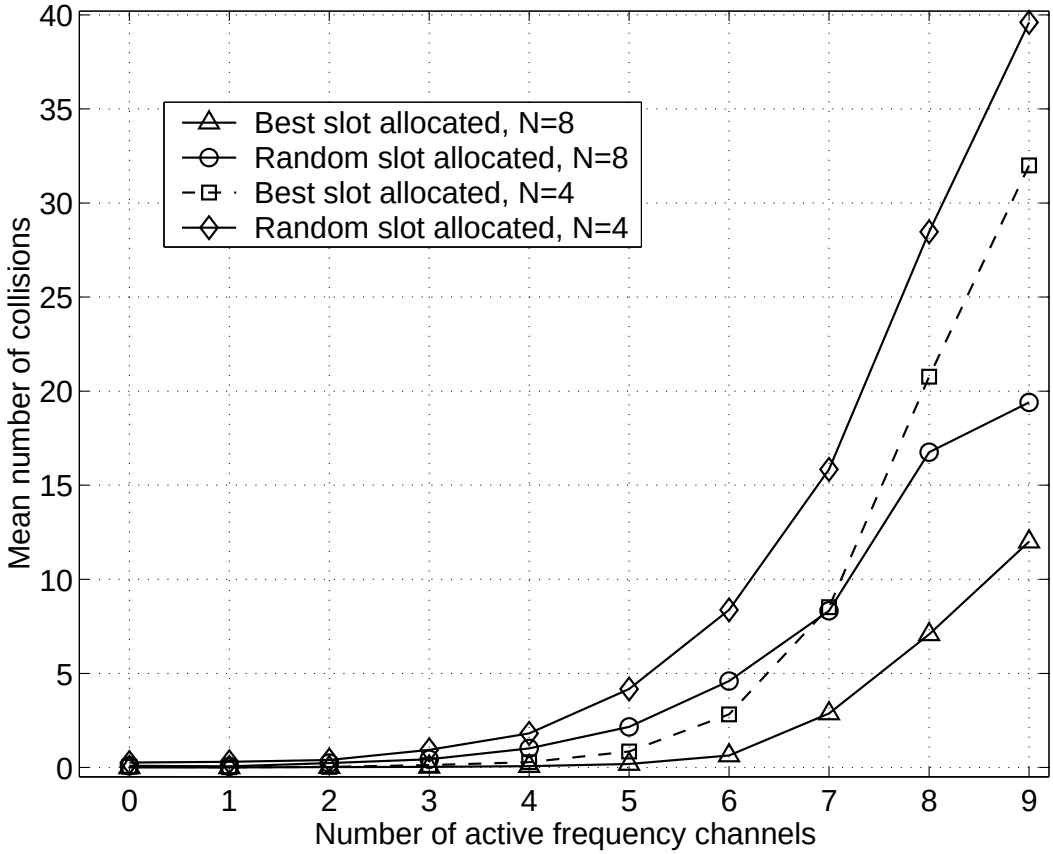

Figure 4: Estimated value of $E\{C|m\}$, the mean number of collisions given m active users using the random frequency channel allocation algorithm and the proposed algorithm for N=4,8. The proposed algorithm reduces the number of collisions and hence, reduces the IMD power at the mobiles.

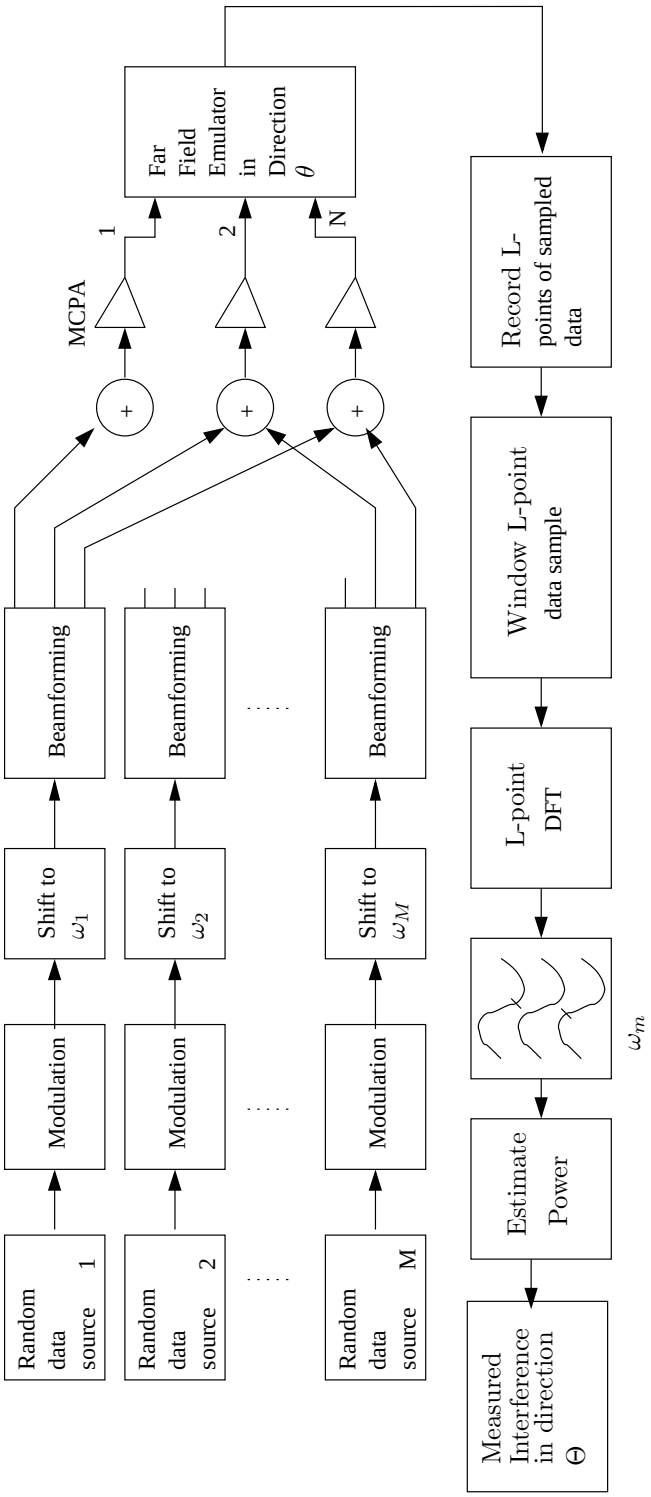

Figure 5: Set up for simulation to evaluate distortion in unoccupied channel in direction Θ

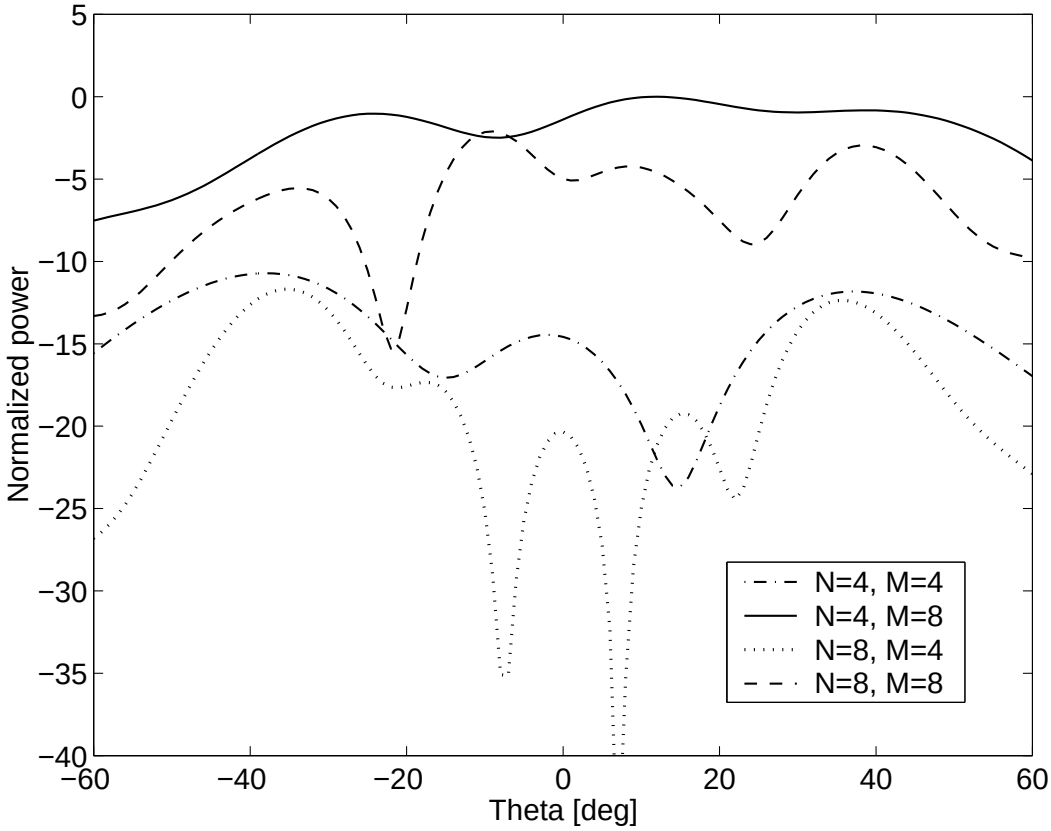

Figure 6: Simulated intermodulation radiation pattern using the power amplifier nonlinearity normalized to a common reference. The reference is defined as the power in the direction of maximum power in the $M = 8$ carrier, $N = 4$ beam case. When the number of beams N is decreased and the number of active frequency channels M is maintained constant, the radiation pattern approaches the single element antenna radiation pattern.

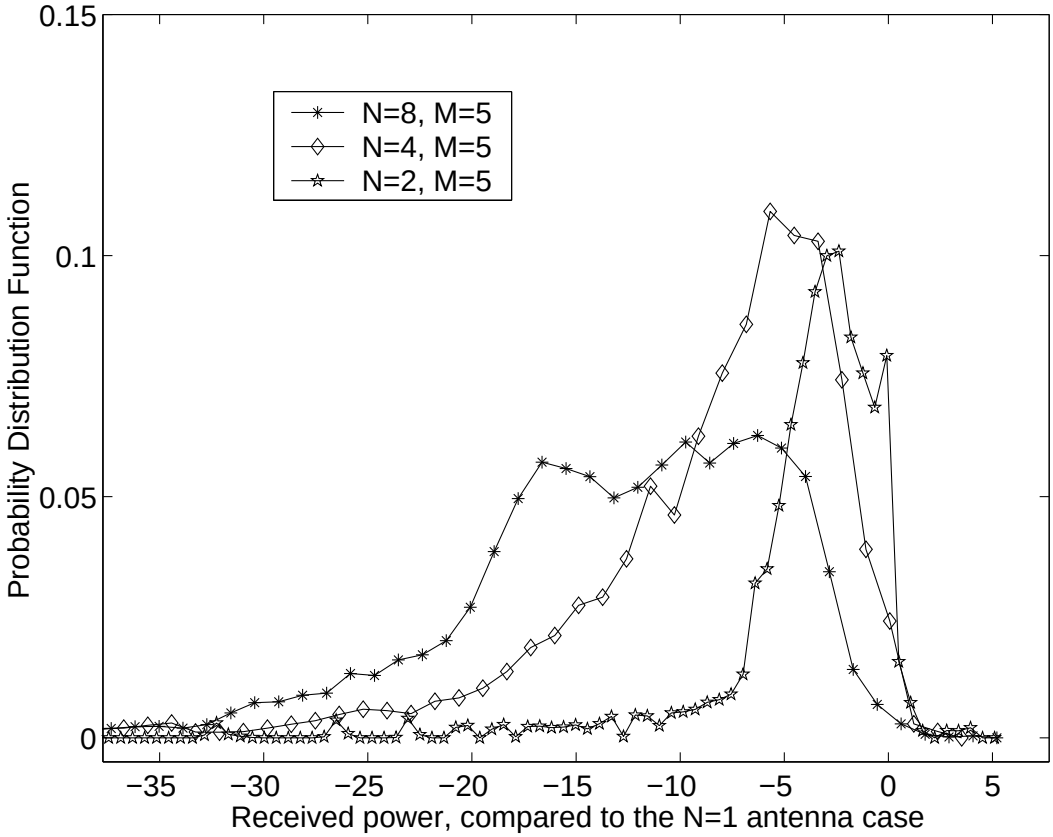

Figure 7: Probability distribution function of the difference in received power in the empty center channel for N antennas, for all angles in the sector. N=1 antenna case is set as a reference. Here, M=5 channels are used.

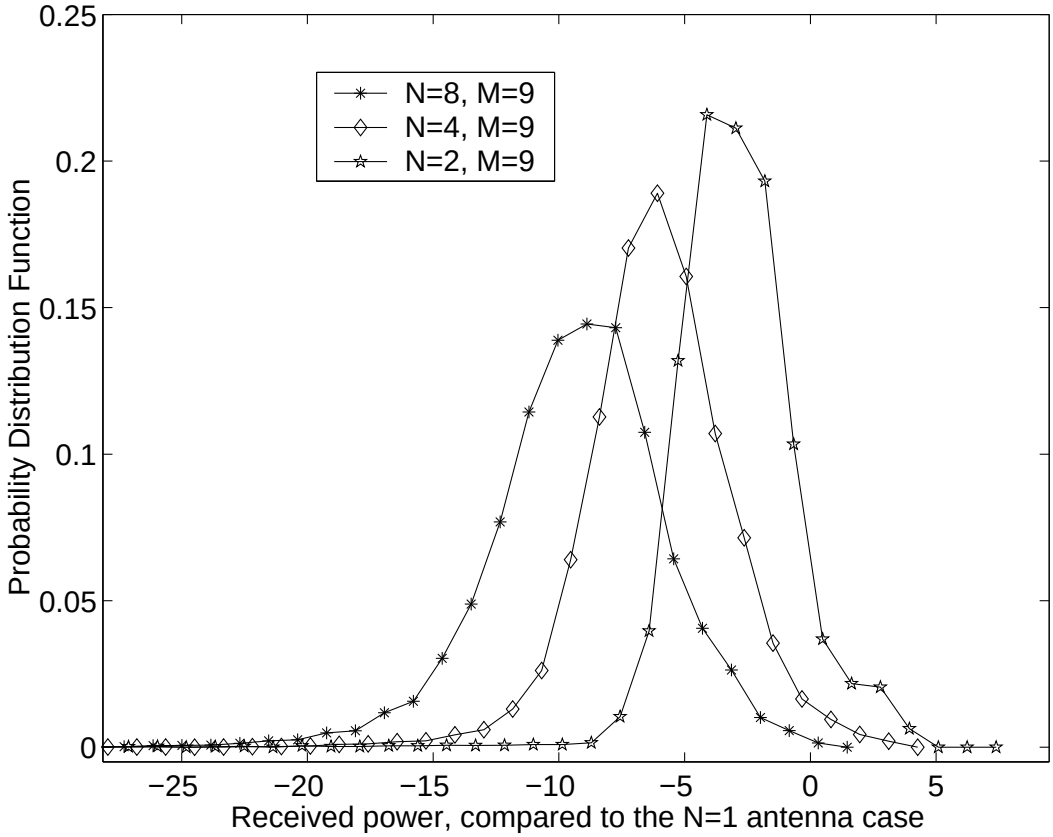

Figure 8: Probability distribution function of the difference in received power in the empty center channel for N antennas, for all angles in the sector. N=1 antenna case is set as a reference. Here, M=9 channels are used.

List of Tables

Table 1: Estimated number of collisions when using proposed algorithm for frequency channel allocation compared to random allocation.

Antennas N	Channel Allocation	Estimated $E\{C\}$
8	Best	0.41
8	Random	2.15
4	Best	1.42
4	Random	4.02
2	Best	4.24
2	Random	8.12
1	Best	10.70
1	Random	16.19

Table 2: Mean of the received power in the empty measurement channel. Reference is the N=1 antenna case.

Antennas N	Channels M	Mean [dB]
8	9	-9.2
8	5	-13.5
4	9	-6.1
4	5	-8.9
2	9	-2.9
2	5	-4.1